

Mitochondria-derived peptide SHLP2 regulates energy homeostasis through the activation of hypothalamic neurons

Received: 7 September 2022

Accepted: 10 July 2023

Published online: 19 July 2023

 Check for updates

Seul Ki Kim^{1,2}, Le Trung Tran^{1,2}, Cherl NamKoong³, Hyung Jin Choi^{3,4}, Hye Jin Chun⁵, Yong-ho Lee⁵, MyungHyun Cheon⁶, ChiHye Chung⁶, Junmo Hwang⁷, Hyun-Ho Lim⁷, Dong Min Shin^{1,2}, Yun-Hee Choi¹ & Ki Woo Kim^{1,2} ✉

Small humanin-like peptide 2 (SHLP2) is a mitochondrial-derived peptide implicated in several biological processes such as aging and oxidative stress. However, its functional role in the regulation of energy homeostasis remains unclear, and its corresponding receptor is not identified. Hereby, we demonstrate that both systemic and intracerebroventricular (ICV) administrations of SHLP2 protected the male mice from high-fat diet (HFD)-induced obesity and improved insulin sensitivity. In addition, the activation of pro-opiomelanocortin (POMC) neurons by SHLP2 in the arcuate nucleus of the hypothalamus (ARC) is involved in the suppression of food intake and the promotion of thermogenesis. Through high-throughput structural complementation screening, we discovered that SHLP2 binds to and activates chemokine receptor 7 (CXCR7). Taken together, our study not only reveals the therapeutic potential of SHLP2 in metabolic disorders but also provides important mechanistic insights into how it exerts its effects on energy homeostasis.

Mitochondria are unique organelles of mammalian cells that possess their own distinct circular mitochondrial DNA (mtDNA). This DNA is known to contain 37 genes that encode 2 rRNAs, 22 tRNAs, and 13 polypeptide subunits of the oxidative phosphorylation (OXPHOS) enzyme complexes¹. Recent studies have identified that mtDNA contains additional short open reading frames (sORFs)² that encode several small regulatory peptides². These peptides are collectively named mitochondrial-derived peptides (MDPs)³. Increasing evidence indicates that MDPs are widely distributed in various tissues throughout the body and play crucial roles in numerous biological activities^{3–5}.

One of the first MDPs discovered is Humanin, a 24-amino-acid peptide encoded by the mitochondrial 16S ribosomal RNA (rRNA)

gene. It was originally identified in 2001 during a screening for neuroprotective factors against Alzheimer's disease^{6,7}. A number of subsequent studies over the past two decades have extensively demonstrated the cytoprotective and beneficial metabolic effects of humanin^{3,5,8}. Another MDP called Mitochondrial Open Reading Frame of the 12S rRNA-c (MOTS-c) is encoded by the mitochondrial 12S rRNA gene⁹. MOTS-c is a mitochondria-originated metabolic hormone which regulates cellular metabolism and promotes energy homeostasis⁹. MOTS-c is also known to communicate with the nuclear genome to modulate nuclear gene expressions under metabolic stress¹⁰ and it acts as an exercise-induced factor to enhance physical capacity¹¹. Moreover, it has been shown that humanin and MOTS-c promote lifespan, while

¹Division of Physiology, Department of Oral Biology, Yonsei University College of Dentistry, Seoul 03722, Korea. ²Department of Applied Life Science, BK21 FOUR, Yonsei University College of Dentistry, Seoul 03722, Korea. ³Neuroscience Research Institute, Seoul National University College of Medicine, Seoul 03080, Korea. ⁴Department of Biomedical Sciences, Seoul National University College of Medicine, Seoul 03080, Korea. ⁵Department of Internal Medicine, Yonsei University College of Medicine, Seoul 03722, Korea. ⁶Department of Biological Sciences, Konkuk University, Seoul 05029, Korea. ⁷Neurovascular Unit Research Group, Korea Brain Research Institute (KBRI), Daegu 41068, Korea. ✉e-mail: kiwoo-kim@yuhs.ac

their plasma levels tend to decline with age^{8,11}. This suggests that the MDPs are also potential therapeutic targets for numerous age-related metabolic disorders.

In addition to humanin and MOTS-c, a recent study has identified an additional six small humanin-like peptides (SHLP1 to 6) encoded by the 16S rRNA gene of the mtDNA genome⁴. Among these, SHLP2 has been reported to have cytoprotective and metabolic effects in mouse models, suggesting that there may exist a potential receptor for SHLP2 in mice^{4,12,13}. Moreover, while both SHLP2 and SHLP3 have been shown to enhance cellular differentiation and insulin sensitivity in adipocytes in vitro, only SHLP2 was found to improve insulin action in vivo⁴. However, the mechanism by which SHLP2 affects whole-body energy homeostasis has not been investigated. Furthermore, the cellular receptor for SHLP2 and its primary site of action have not been identified.

In the present study, we discovered that serum SHLP2 levels were significantly lower in obese and diabetic patients compared to healthy individuals. In murine animal models, administration of SHLP2 resulted in the suppression of food intake, activation of thermogenesis, and prevention of diet-induced obesity. Additionally, a combination of experimental approaches, including patch-clamp techniques and the designer receptors exclusively activated by designer drugs (DREDD) system, revealed that POMC neurons in the hypothalamic ARC are necessary for the SHLP2-induced suppression of food intake and increased energy expenditure (EE). Using high-throughput structural complementation screening, we identified a potential receptor for SHLP2.

Results

Serum SHLP2 levels are decreased in obese and diabetic patients

SHLP2 is associated with insulin sensitivity in mice⁴. This prompted us to investigate whether the serum SHLP2 levels might be altered by metabolic disease conditions in human. To answer this question, we first developed a polyclonal antibody for SHLP2 and validated its specificity (Supplementary Fig. 1a–c). In addition, our antibody was able to specifically detect SHLP2 without any cross-reactivity with other SHLPs, highlighting its high specificity for SHLP2 (Supplementary Fig. 1d). Subsequently, we conducted dot blot analyses using human sera collected from normal, obese, and diabetic subjects (Supplementary Table 1). Interestingly, we observed a significant decrease in serum levels of SHLP2 in both diabetic and obese patients compared to healthy individuals (Fig. 1a). The decreased levels of serum SHLP2 were also observed in murine obesity and diabetic models, such as *ob/ob* and *db/db* mice (Supplementary Fig. 1e), indicating that the serum levels of SHLP2 may be influenced by individual metabolic conditions.

SHLP2 protects mice from diet-induced metabolic syndrome

To investigate the metabolic effects of SHLP2, we administered various doses of SHLP2 intraperitoneally (IP) and identified the effective dose (2 mg/kg, IP) for acute suppression of food intake (Supplementary Fig. 2a). At this dose, SHLP2 exhibited the unique ability to suppress rebound food intake and body weight gain for up to 8 h after refeeding, as compared to scrambled peptides, highlighting the specific role of SHLP2 in regulating energy homeostasis (Supplementary Fig. 2b, c). Nonetheless, under normal chow (NC) conditions, SHLP2 only exhibited a tendency to decrease food intake and body weight (Supplementary Fig. 2d–f). Notably, when SHLP2 was injected daily for 3 weeks, it improved glucose tolerance and insulin sensitivity, suggesting its intrinsic effects on insulin sensitivity independent of body weight (Supplementary Fig. 2g, h).

In contrast to NC, SHLP2 significantly protected mice against diet-induced body weight gain in high-fat diet (HFD) conditions (Fig. 1b). In addition, SHLP2 injection decreased total body fat mass and circulating leptin levels (Fig. 1c, d). Histological analysis further revealed a

significant reduction in the size of inguinal and epididymal white adipose tissues (WAT), as well as a profound decrease in HFD-induced hepatic steatosis, as evidenced by decreased intracellular lipid droplets and reduced expression of lipogenic genes in hepatocytes (Fig. 1e–h). Moreover, the administration of SHLP2 resulted in a significant lowering of blood glucose levels and improved glucose tolerance and insulin sensitivity (Fig. 1i–k). Taken together, these results demonstrated that the systemic SHLP2 administration protects mice against HFD-induced obesity and metabolic disorders.

SHLP2 suppresses food intake and promotes thermogenesis

To understand the underlying mechanisms of how SHLP2 influences metabolism, we utilized indirect calorimetry to assess metabolic parameters following a four-week period of systemic SHLP2 administration. Systemic SHLP2 administration robustly increased O₂ consumption (VO₂), CO₂ production (VCO₂) as well as heat generation without alteration in the physical activities (Fig. 2a–d). Given that the interscapular brown adipose tissue (iBAT) is a well-known organ for thermogenesis, primarily through the action of uncoupling protein 1 (UCP1)¹⁴, we further examined the thermogenic effect of SHLP2 in the iBAT. SHLP2 markedly up-regulated *Ucp1*, as well as the genes involved in iBAT thermogenesis including *Pgc1a*, *Dio2*, *Prdm16*, and *Nrf1* (Fig. 2e). Moreover, the iBAT of SHLP2-administered mice displayed a decrease in lipid vacuoles, an increase in UCP1 protein levels, and a higher mitochondrial content compared to mice injected with saline (Fig. 2f, g). The increase in iBAT thermogenesis in the SHLP2-injected mice may be attributed to an increase in sympathetic tone directed to the iBATs. This was proven by the elevation of plasma norepinephrine (NE) level and the activation of the cAMP response element-binding protein (CREB) and p38 MAPK, which are the downstream effectors of the β₃-adrenergic receptor signaling in the iBATs (Fig. 2h, i)¹⁵. In addition to a notable increase in EE, mice treated with SHLP2 showed a significant reduction in daily food intake (Fig. 2j). This decrease in food intake was linked to a reduction in the expression of orexigenic neuropeptides, including agouti-related peptide (*Agrp*) and neuropeptide Y (*Npy*), in the hypothalamus (Fig. 2k). These results indicate that systemic administration of SHLP2 prevented the diet-induced obesity through an enhanced thermogenesis and a decrease in energy uptake.

SHLP2 activates the hypothalamic neurons

The diverse effects of SHLP2 on iBAT thermogenesis, elevated serum NE levels, as well as its anorexigenic impact by modulating hypothalamic neuropeptides, suggested that the CNS could potentially serve as a target site for SHLP2 and play a crucial role in its metabolic effects. To investigate whether SHLP2 can directly reach the CNS, we systemically injected SHLP2 or saline and probed for SHLP2 in the cerebrospinal fluid (CSF). Remarkably, SHLP2 was highly detected in the CSF of SHLP2-administered mice (Fig. 3a). Next, we evaluated c-Fos immunoreactivity in various brain regions following systemic injection of SHLP2. The results showed that the mediobasal hypothalamus, a major region in the brain that regulates metabolic homeostasis, exhibited the highest c-Fos activation (Fig. 3b, c)^{16,17}. Analysis of c-Fos immunoreactivity throughout the mediobasal hypothalamus revealed a significant increase in the arcuate nucleus (ARC) and dorsomedial hypothalamus (DMH) in the SHLP2-injected mice, while no differences were observed in the ventromedial nucleus (VMH) and lateral hypothalamus (LH) between the saline and SHLP2 groups (Fig. 3b–d). In contrast to the hypothalamus, we did not observe any significant changes in c-Fos activation in other brain regions such as the cortex, hippocampus, and periaqueductal gray (PAG) following systemic administration of SHLP2 (Supplementary Fig. 3a–c). The ICV administration of SHLP2 into the third ventricle (3V) showed similar results with distinct c-Fos activation mainly in the ARC and DMH (Fig. 3e, f). These findings suggested that SHLP2 could cross the brain-CSF barrier and directly activate hypothalamic neurons.

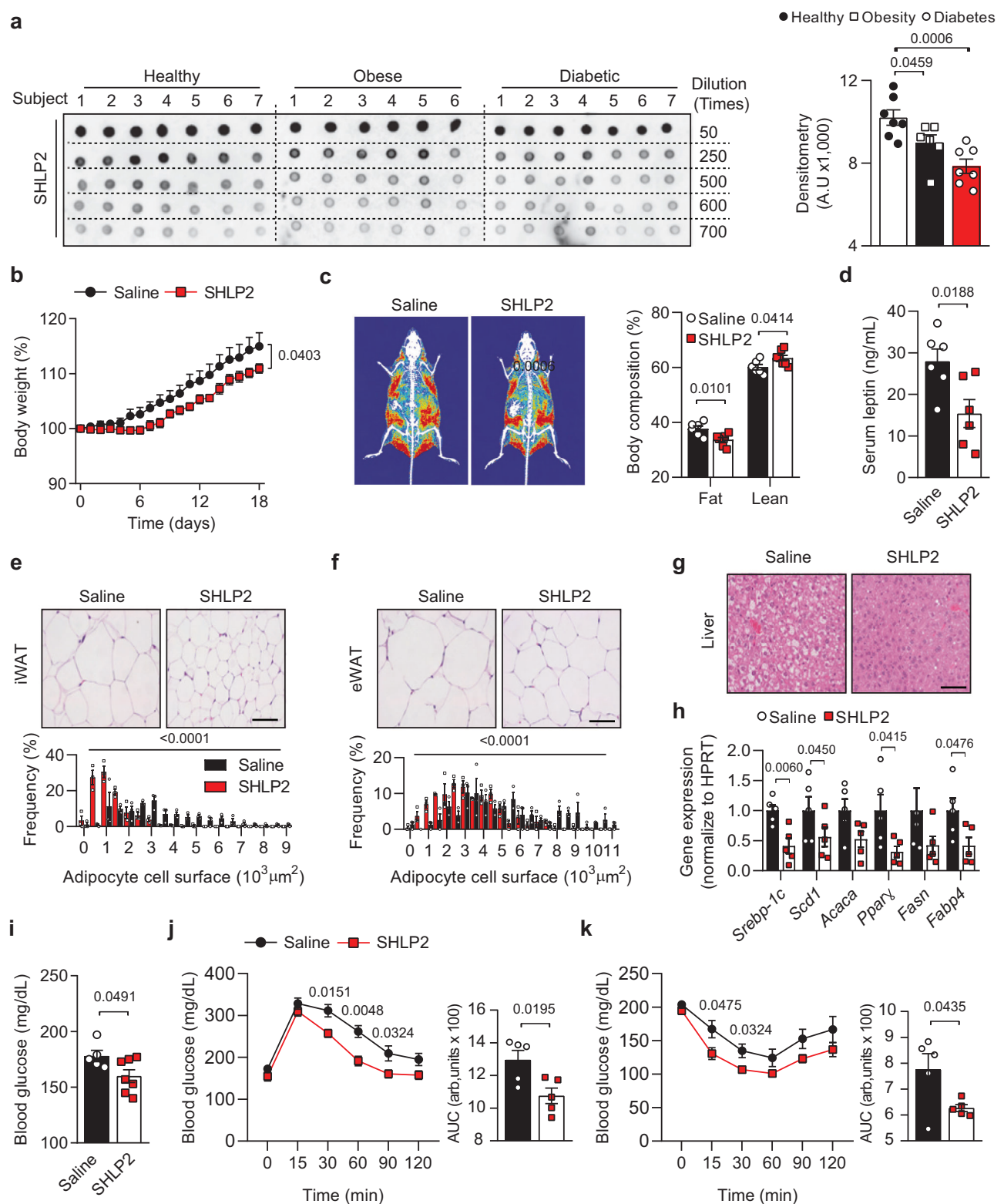


Fig. 1 | Protective effect of SHLP2 from HFD-induced obesity. **a** Dot-blot image (left) and relative blot densitometry (right) detecting plasma SHLP2 levels in healthy ($n=7$), obese ($n=6$), and diabetic ($n=7$) male subjects. **b** Change of body weight (%) in male mice fed with HFD after daily intraperitoneal (IP) injection of saline or SHLP2 for 3 weeks ($n=9$ saline, $n=11$ SHLP2). **c** Representative DEXA images (left) and body composition (right) ($n=6$ saline, $n=7$ SHLP2). **d** Serum leptin levels ($n=6$ each group). **e**, **f** Representative adipose tissues images from iWAT (**e**) and eWAT (**f**) ($n=3$). Frequency distribution of adipocytes from iWAT and eWAT samples (bottom graphs). **g** Representative liver images ($n=3$). **h** Expression

of lipogenic genes in liver ($n=5$ each group). **i** Blood glucose levels in fed condition ($n=5$ saline, $n=7$ SHLP2). **j**, **k** GTT (**j**) and ITT (**k**) were performed in HFD-fed male mice before body weight divergence following IP administration of either saline or SHLP2 ($n=5$ each group). Scale bars, 50 μm . n indicates the number of biologically independent human subjects or animals examined. Data were presented as mean \pm SEM. Two-tailed Student's t tests were used in (**a**), (**c**–**k**), and two-way ANOVA with Bonferroni post-hoc tests were used in (**b**). Source data are provided as a Source Data file.

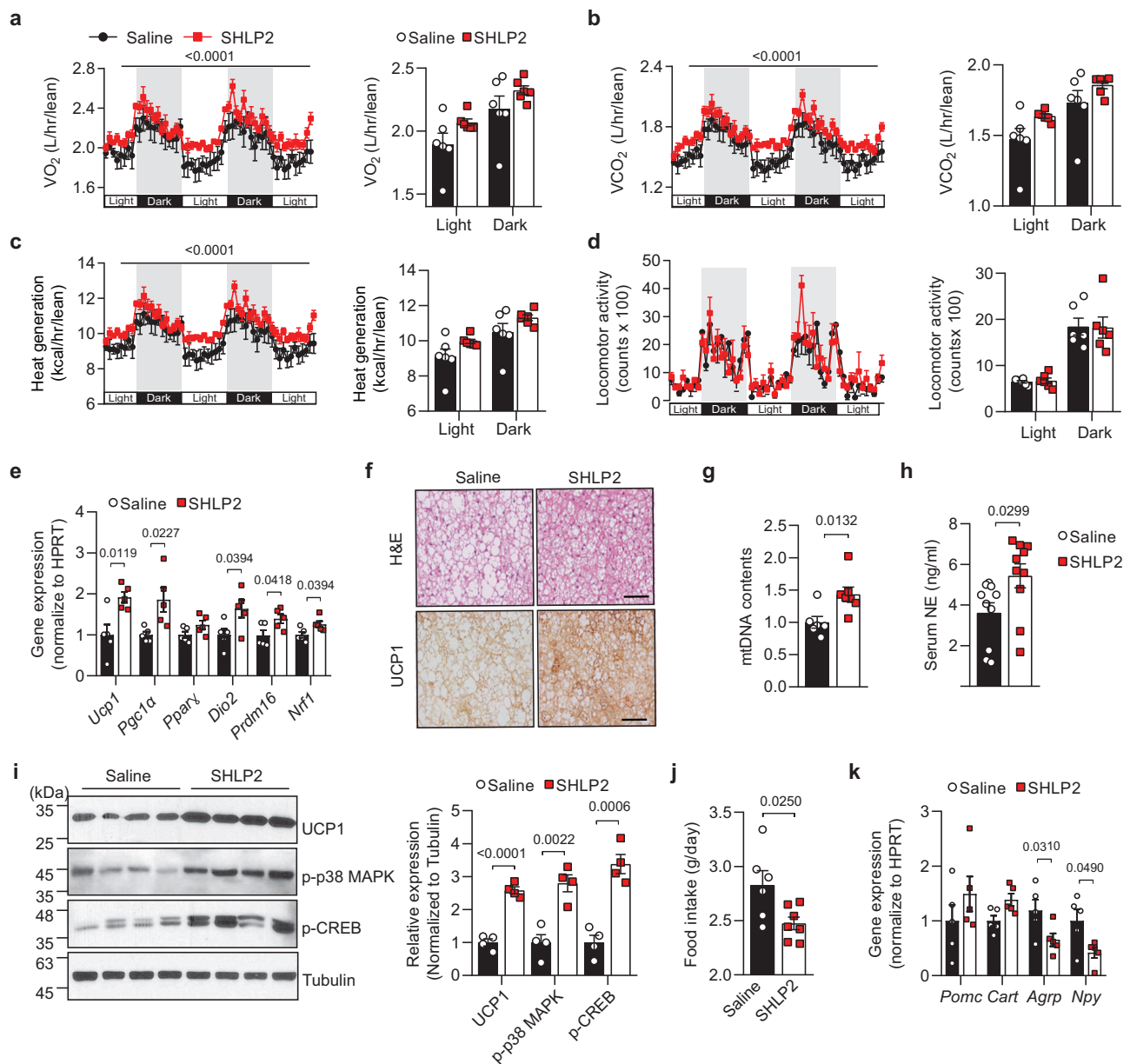


Fig. 2 | SHLP2 enhances iBAT thermogenesis and suppresses energy intake.

a–d Temporal changes (left) and average values (right) of O_2 consumption (**a**), CO_2 production (**b**), heat generation (**c**), and locomotor activity (**d**) from HFD-fed male mice with IP administration of either saline or SHLP2 ($n = 6$ each group). **e** Expression of thermogenic genes in iBAT from indicated groups ($n = 5$ each group). **f** Representative H&E (top) and UCP1 (bottom) staining from iBAT of HFD-fed male mice ($n = 3$ each group). **g** Mitochondrial DNA contents in the iBAT ($n = 6$ saline, $n = 7$ SHLP2). **h** Serum norepinephrine (NE) levels in indicated group ($n = 10$ each group). **i** Immunoblots (left) and relative densitometry (right) of UCP1,

p-p38 MAPK, p-CREB expression in the iBAT samples ($n = 4$ each group). Data shown are representative of three independent experiments with similar results. **j** Daily food intake of HFD-fed male mice treated with either saline or SHLP2 ($n = 6$ saline, $n = 7$ SHLP2). **k** Gene expression of neuropeptides regulating feeding in the hypothalamic samples ($n = 5$ each group). Scale bars, $50 \mu\text{m}$. n indicates the number of biologically independent animals examined. Data were presented as mean \pm SEM. Two-tailed Student's t tests were used in bar graphs, and two-way ANOVA with Bonferroni post-hoc tests were used in line graphs. Source data are provided as a Source Data file.

Central SHLP2 administration improved energy homeostasis

Based on the aforementioned results, we hypothesized that SHLP2 directly affects hypothalamic neuronal circuits and whole-body energy homeostasis. To examine this possibility, we administered SHLP2 directly into the 3V and assessed metabolic changes (Supplementary Fig. 4a). Following analysis of dose responses, we determined that a $3 \mu\text{g}$ was appropriate for ICV injection (Supplementary Fig. 4b, c). Interestingly, a single ICV injection of SHLP2 produced a suppressive impact on food intake and body weight gain for up to three days, in both NC and HFD-fed states (Fig. 4a, b, and Supplementary Fig. 4d–f). Following ICV administration of SHLP2, a consistent increase in EE was observed without any change in locomotor activity, even in NC-fed

conditions (Fig. 4c–f). The expression of thermogenic genes and UCP1 was significantly enhanced in iBAT (Fig. 4g, h). Additionally, SHLP2 improved glucose tolerance and exhibited a strong trend towards increasing insulin sensitivity (Fig. 4i, j and Supplementary Fig. 4g, h). These results strongly indicate that the thermogenic and anorexigenic effects of SHLP2 might be mediated through the CNS.

Activation of POMC neurons is involved in the anti-obesity effect of SHLP2

To investigate which neuronal populations are responsible for the anorexigenic and thermogenic effects of SHLP2, we monitored POMC and AgRP neurons in the ARC, which regulate food intake and EE^{18–20}.

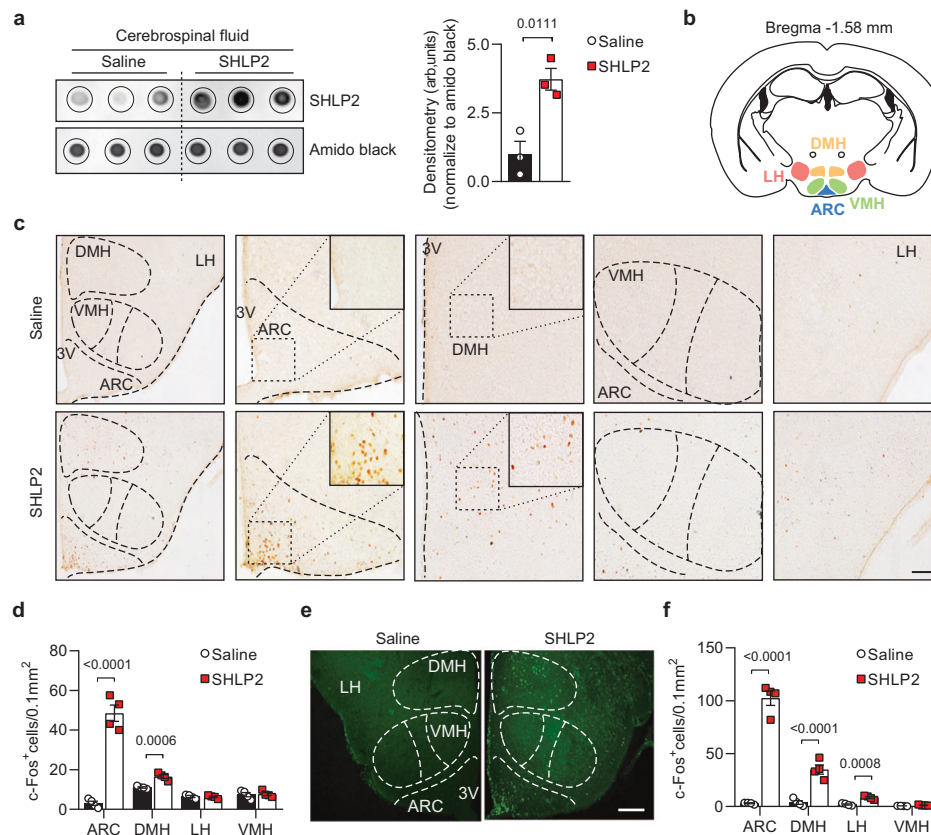


Fig. 3 | SHLP2 induces c-Fos activation in hypothalamic neurons. **a** Dot blots (left) for SHLP2 and their relative densitometry (right) in CSF after an IP injection of saline or SHLP2 ($n = 3$ each group). **b**, **c** c-Fos immunoreactivity in mediobasal hypothalamic nuclei after an IP injection of saline or SHLP2. **d** Quantification of c-Fos activities from (c) ($n = 4$ each group). **e**, **f** Representative figures (e) and graph

quantification (f) of c-Fos immunoreactivity in hypothalamic regions after an ICV administration of saline or SHLP2 ($n = 4$ each group). Scale bars, 100 μm . n indicates the number of biologically independent animals examined. Data were presented as mean \pm SEM. Two-tailed Student's t tests were used in bar graphs. Source data are provided as a Source Data file.

Following SHLP2 administration, we monitored c-Fos activation in POMC or AgRP neurons using POMC-Cre or AgRP-ires-Cre mice with the Cre-dependent reporter tdTomato, allowing for the visualization of POMC and AgRP neurons, respectively (tdTomato^{POMC-Cre} or tdTomato^{AgRP-Cre} mice)^{20–23}. Upon ICV injection of SHLP2, c-Fos expression was primarily observed in POMC neurons (51.4%) as opposed to AgRP neurons (22.8%) (Fig. 5a and Supplementary Fig. 5a). Subsequently, whole-cell patch clamp experiments were conducted on POMC neurons to further examine the effects of SHLP2 on their activity (Fig. 5b–e). In response to SHLP2 (1 μM), 34.49% of POMC cells (10 out of 29) were depolarized, resulting in a mean change of $+4.43 \pm 2.31$ mV in the resting membrane potential (Fig. 5b–e). The depolarized POMC cells were distributed across the mediobasal hypothalamus and were clustered near the 3V (Supplementary Fig. 5b). Interestingly, the depolarization of POMC neurons induced by SHLP2 was not affected by the presence of synaptic blockers such as TTX, picrotoxin, CNQX, and D-AP-5 in the bath solution, as evidenced by an increase in resting membrane potential by $+3.17 \pm 0.17$ mV in 4 out of 8 tested cells (Fig. 5f, g). However, the SHLP2 application resulted in only a minor suppression of AgRP neuron activity (Supplementary Fig. 5c, d). These results strongly suggest that SHLP2 directly activates POMC neurons while marginally inhibiting AgRP/NPY neurons.

To further confirm the significance of POMC neuronal activation in the metabolic effects mediated by SHLP2, we employed two different DREADD systems. First, we performed stereotaxic injection of adeno-associated virus (AAV) that expressed either a Cre-dependent mCherry (pAAV-mCherry) or an mCherry reporter fused with the hM4Di receptor (pAAV-hM4D(Gi)-mCherry) into the hypothalamus of

POMC-Cre mice. This allowed us to generate POMC-mCherry or POMC-hM4Di mice. Second, we produced mice that selectively expressed the hM4Di receptor solely in POMC neurons (hM4Di^{POMC-Cre}) by crossing POMC-Cre mice with mice that carried the floxed hM4Di allele^{21,24}. By utilizing these two distinct methods, we were able to selectively suppress the activity of POMC neurons through treatment with Clozapine-N-oxide (CNO) (Fig. 5h, i and Supplementary Fig. 5e–i). Control mice with intact POMC neurons, such as POMC-mCherry and hM4Di^{f/f}, demonstrated a significant decrease in rebound food intake and body weight gain upon ICV administration of SHLP2 (Fig. 5j, k and Supplementary Fig. 5j, k). However, when POMC neuron activity was blocked by CNO treatment in the POMC-hM4Di and hM4Di^{POMC-Cre} mice, the suppressive effects of energy intake by SHLP2 were notably blunted (Fig. 5j, k and Supplementary Fig. 5j, k). The thermogenic effects of SHLP2 were evident in control mice, as demonstrated by the marked increase in skin and rectal temperature. Nonetheless, inhibiting POMC neurons compromised these SHLP2-induced thermogenic effects (Fig. 5l–n). The results support the involvement of hypothalamic POMC neurons in the regulation of food intake and energy expenditure mediated by SHLP2.

The chemokine receptor CXCR7 mediates effects of SHLP2

To identify the cellular receptor(s) responsible for SHLP2 activity, we conducted a screening using the cell-based PathHunter β -Arrestin assay [<https://www.discoverx.com>]. This assay is capable of monitoring GPCR activation in a homogeneous and non-imaging manner, utilizing enzyme fragmentation complementation with β -galactosidase as the functional reporter. A total of 168 known GPCRs were screened²⁵.

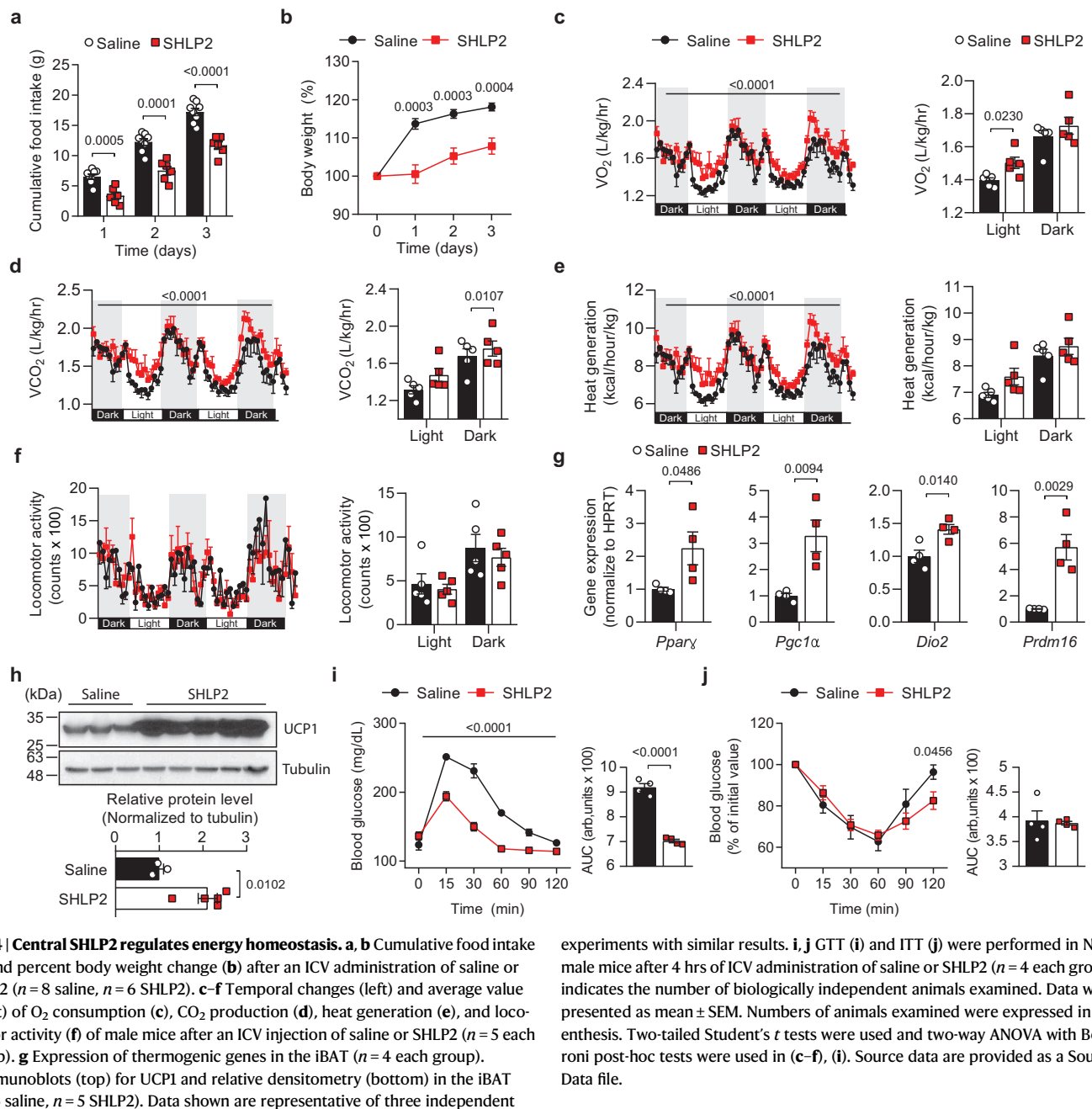


(Fig. 6a). Out of the screened GPCR candidates, SHLP2 showed the highest efficiency in recruiting β -Arrestin to the chemokine receptor CXCR7 (previously known as ACKR3). The relative agonistic activity of SHLP2 was approximately 70% of its known ligand, stromal cell-derived factor-1 (SDF1 α)/CXCL12 (Fig. 6b and Source Data Fig. 6b). By applying the same experimental paradigm, we found that SHLP2 induced β -Arrestin recruitment to CXCR7 in a dose-dependent manner, with a half maximal effective concentration (EC_{50}) of 0.9696 μ M (Fig. 6c). Additionally, the SHLP2 binds directly to CXCR7, as evidenced by the detection of tagged CXCR7 through pulldown analysis (Fig. 6d). The SHLP2 has a specific effect on the CXCR7 chemokine receptor, causing its internalization, without affecting CXCR4 (Supplementary Fig. 6a–g). This suggests that SHLP2 has a selective affinity for CXCR7, and it could potentially activate distinct signaling pathway through this receptor. The interaction between SHLP2 and CXCR7 was further confirmed using the Nanoluc-complementation system, which

demonstrated the recruitment of β -Arrestin to CXCR7²⁶ (Fig. 6e). SHLP2-induced recruitment of β -Arrestin to CXCR7 was comparable to the known ligand CXCL12 at a concentration 50 ng/mL (Fig. 6f).

CXCR7 is known to activate the MAP Kinase - ERK1/2 signaling cascade by recruiting β -Arrestins upon ligand binding^{27–29}. Thus, the SHLP2 could potentially induce ERK1/2 phosphorylation and subsequently increase the excitation of POMC neurons^{30,31}. Indeed, the SHLP2 treatment resulted in strong phosphorylation of ERK1/2 in vitro (Fig. 6g). To confirm the necessity of ERK signaling for the depolarizing effect of SHLP2 on POMC neurons, acute hypothalamic slices were pre-incubated with the MAP kinase blocker PD98059 after confirming CXCR7 expression in the neurons (Supplementary Fig. 6h). The blockage of MAPK/ERK signaling abolished the SHLP2-induced depolarization of all recorded POMC neurons (Fig. 6h, i, k). On the other hand, blocking PI3K, which is a converging point for many peptides and hormones on POMC neurons³², did not affect the depolarizing

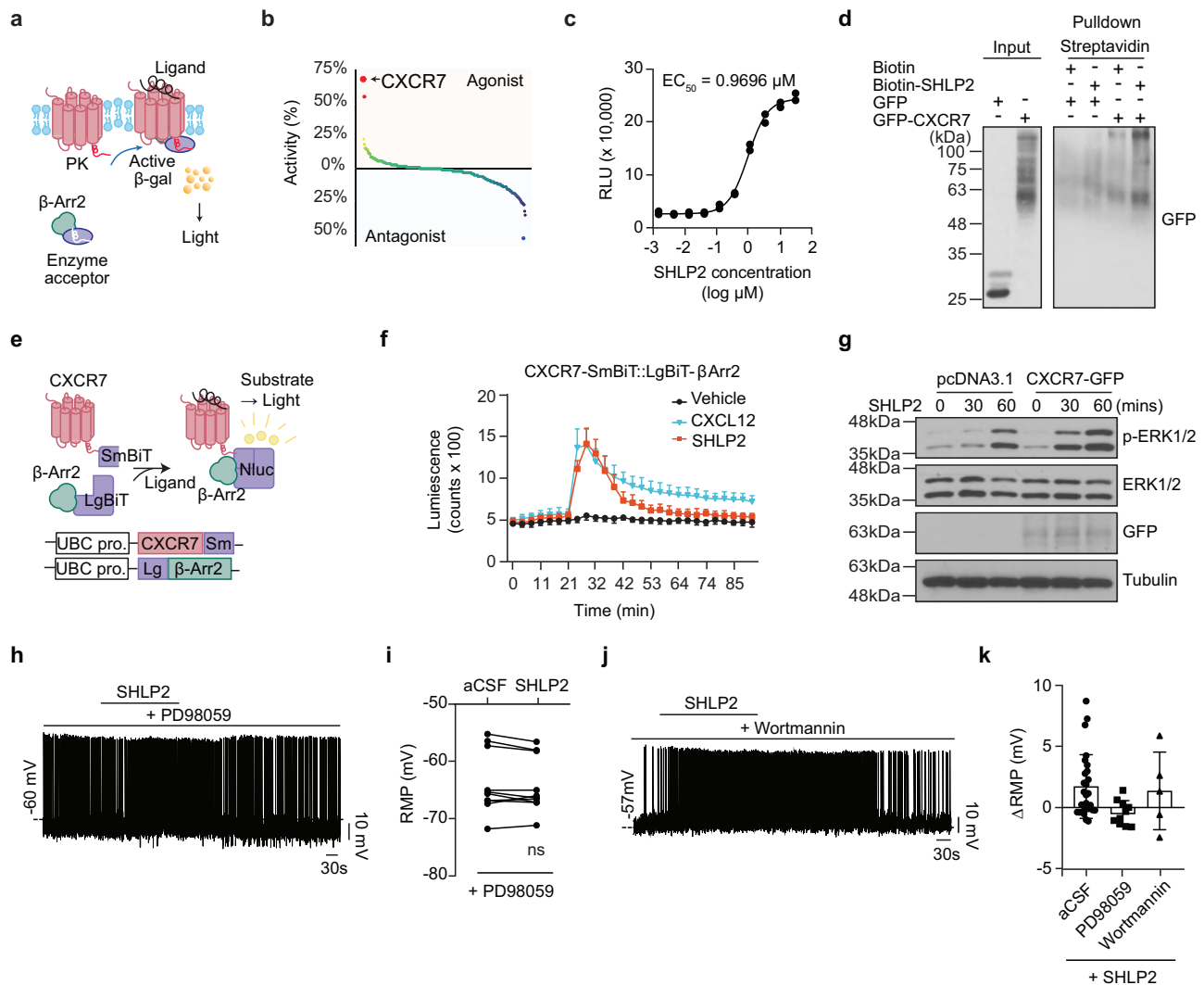


Fig. 6 | Chemokine receptor CXCR7 interacts with SHLP2. **a** Schematic for PathHunter β -Arrestin assay. **b** Activity plot showing the results of PathHunter β -Arrestin GPCR screening. Note that CXCR7 exhibited the highest activity by SHLP2. **c** Dose-dependent β -Arrestin recruitment to CXCR7 by SHLP2. The concentration of SHLP2 inducing half-maximal response (EC_{50}) was calculated by least-square fitting to a four-parameter logistic curve. **d** Pull-down analysis of streptavidin-SHLP2-biotin showing the interaction between SHLP2 and CXCR7. Data shown are representative of five independent experiments with similar results. **e** Schematic (upper panel) and the plasmid DNA (lower panel) of the NanoBiT complementation assay to monitor SHLP2-induced β -Arrestin2 recruitment to CXCR7. **f** Results of β -Arrestin2 recruitment to CXCR7 by SHLP2 or CXCL12 ($n = 4$). **g** Western blot result of time-dependent ERK1/2 phosphorylation by SHLP2 with or without CXCR7 overexpression. Data shown are representative of five independent experiments

with similar results. **h** Representative spike of POMC neuron showing the depolarization by SHLP2 is blocked by the pretreatment of the MAP Kinase blocker PD98059. **i** Summary graph of SHLP2 effect on the resting membrane potential (RMP) of POMC neurons under treatment of the MAP Kinase blocker ($n = 10$ from 4 animals; ns: not significant, paired t test). **j** Representative depolarizing response of POMC neurons by SHLP2 under treatment of the PI3K inhibitor wortmannin. **k** Summary graph showing the changes in resting membrane potential (Δ RMP) by SHLP2 treatment with or without MAP Kinase or PI3K inhibitor ($n = 27, 10, 5$, respectively). n indicates the number of biologically independent cells examined. Data are presented as the mean \pm SD. PK, enzyme donor fragment ProLink; β -Arr2, β -Arrestin2; β -gal, β -galactosidase; Nluc Nano Luciferase, SmBiT Small fragment, LgBiT Large fragment, UBC pro UBC promoter. Source data are provided as a Source Data file.

brain-CSF barrier and activate the POMC neurons of the ARC, which directly suppressing food intake and promoting thermogenesis. Moreover, our study identified CXCR7 as a cellular receptor for SHLP2, providing detailed insight into the mechanism underlying its pharmacological actions. These findings suggest that SHLP2 may represent a promising therapeutic target for metabolic disorders, and offer potential avenues for the development of effective treatments for these conditions.

Metabolic disorders and other diseases can cause a decline in mitochondrial function, leading to a gradual loss of MDP expressions and potentially reducing their functions^{33–35}. Our findings suggest that this may also be the case for SHLP2, as we observed decreased serum levels of SHLP2 in both diabetic and obese patients, indicating that it

may have a preventative role in human metabolic diseases (Fig. 1a). Animal models of diabetes or obesity, such as *db/db* and *ob/ob* mice, also exhibited decreased levels of SHLP2, further supporting this hypothesis. Several previous reports supported the notion that the MDPs might play important roles in preventing several diseases. For example, humanin was decreased in human diseases such as Alzheimer's disease, mitochondrial encephalopathy, lactic acidosis, and stroke-like episodes⁸. In addition, the circulating MOTS-c was reduced in diabetes patients³⁶. Interestingly, circulating SHLP2 was decreased in aged mice, implying that SHLP2 might be involved in the aging process of rodents⁴. Therefore, it would be interesting to explore whether certain MDPs, including SHLP2, can be utilized as diagnostic markers for specific human diseases such as metabolic or age-related disorders.

Following intraperitoneal administration of SHLP2 in mice, there was a reduction in appetite and food intake and an increase in brown fat thermogenesis (iBAT). Moreover, SHLP2 was observed in the cerebrospinal fluid (CSF) and activated c-Fos in multiple hypothalamic neurons, including the arcuate nucleus (ARC), dorsomedial hypothalamus (DMH), and lateral hypothalamus (LH), indicating that the brain could be a potential target for SHLP2's metabolic regulation. Immunohistochemistry and electrophysiological approaches, indeed, identified POMC neurons in the ARC as primary targets for the action of SHLP2. The *ex vivo* patch-clamp experiments revealed that SHLP2 depolarized a subset of hypothalamic POMC neurons, and the activation did not rely on synaptic inputs. Specifically, the fraction of neurons was activated under the treatment of TTX and synaptic blockers, indicating that SHLP2 acted directly on the POMC neurons, independent of synaptic inputs. Further experiments using inhibitory DREADDs targeting POMC neurons confirmed that SHLP2 regulates the hypothalamic melanocortin system. The heterogeneity of POMC neurons in the arcuate nucleus, characterized by different expressions of ion channels and receptors, may result in diverse neuronal responses to hormones and neurotransmitters^{37–39}. Thus, future research identifying ion channels or related receptors responsible for SHLP2-mediated excitability of POMC neurons holds promise for future investigation. Additionally, since activation of POMC neurons has been linked to the regulation of blood pressure and cardiac function⁴⁰, it would be interesting to investigate whether SHLP2 is also involved in the regulation of other intrinsic functions of POMC neurons, such as blood pressure and cardiac function. In contrast to its effect on POMC neurons, SHLP2 slightly inhibited AgRP neurons. Additionally, our observation on SHLP2-induced c-Fos expression in other hypothalamic neuronal populations suggests that SHLP2 may also play a role in regulating other physiological functions in the central nervous system beyond POMC neurons.

The pharmacological action of SHLP2 was further revealed by the identification of CXCR7 as a receptor mediating its action. We used a GPCR screening system to identify potential receptors. The chemokine receptor CXCR7 appeared as a potential receptor for SHLP2. Further characterizations showed that SHLP2 recruits β -Arrestin 2 at the concentration of inducing POMC-neuron activation. CXCR7 and β -Arrestin 2 are known to activate the MAP Kinase–ERK cascade^{28,41}, thus we hypothesized that SHLP2 induced the depolarization of POMC neurons through ERK1/2 phosphorylation. Indeed, the MAP kinase inhibition blunted the effect of SHLP2 on the tested POMC neurons. Although the identification of CXCR7 as the receptor of SHLP2 in activating ERK signaling and POMC neuronal activation is a significant finding, further investigation is necessary to fully understand the exact mechanism of SHLP2. Specifically, additional studies are needed to explore whether SHLP2 affects other signaling pathways in addition to ERK. By investigating broader pharmacological effects of SHLP2, we may gain a more comprehensive understanding of its potential as a therapeutic target for various diseases. Interestingly, previous studies have demonstrated that CXCR7 is involved in the modulation of ER stress in cardiac cells through AMPK activation⁴². This raises a possibility that genetic approaches targeting the CXCR7-encoding *Ackr3* gene (CXCR7 KO) *in vivo* might be a way to elucidate a more complete signaling cascade of CXCR7 and SHLP2. By using genetic approaches, we may be able to better understand the interplay between CXCR7 and other pathways and ultimately develop more effective therapeutic strategies targeting this signaling pathway.

In summary, our current study has demonstrated that the mitochondrial-derived peptide SHLP2 has profound metabolic benefits through its actions on the central nervous system, specifically on POMC neurons in the hypothalamus. In addition, identifying the activation of the chemokine receptor CXCR7 by SHLP2 highlights its potential as a novel therapeutic candidate for the treatment of metabolic diseases.

Methods

Reagents

Small humanin-like peptide 1 to 6 (SHLP1-6) were purchased from AnyGen [<http://www.anygen.com/eng/>]. For each peptide, the Fmoc-Ser (tBu)-Wang resin was allowed to swell in dimethylformamide (DMF). The amino acid was then deprotected using a solution of 20% piperidine in DMF. Coupling was carried out using Hexafluorophosphate Benzotriazole Tetramethyl Uronium (HBTU), *N*-methylmorpholine (NMM) in DMF. Stepwise deprotection and coupling of amino acids was repeated until the desired peptides was synthesized. The peptides were cleaved from dried resin using a trifluoroacetic acid (TFA) solution containing 2.5% 1, 2 ethanedithiol (EDT), 5% thioanisole and 5% distilled water. Crude peptides were precipitated in ether, and dried under vacuum. Peptides were purified using commercial columns (YMC-Triart C18/S-5 $\mu\text{m}/12\text{nm}\cdot 5\mu\text{m}$ (20 x 250 mm) and each fraction was obtained at a flow rate of 1 mL/min. The collected fractions were analyzed via HPLC (Shimadzu HPLC LabSolution) and MALDI-TOF MS (AXIMA Assurance, Shimadzu). The fractions containing the pure peptide were mixed and then lyophilized. SHLP2 were freshly prepared at 1 $\mu\text{g}/\mu\text{L}$ by diluting in saline, and were freshly used for mice. The information of SHLP peptide sequence used in study were listed in Supplementary Table 3.

Antibody generation

Custom rabbit anti-SHLP2 were generated from Ab Frontier [<http://www.younginfrontier.com/laboratory/abfrontier/>]. Two (one for each SHLP2 peptide synthesized from Ab Frontier) healthy New Zealand white rabbits (1.8–2.0 kg, obtained from the Sinyang) were subcutaneously immunized with 1 mL of the prepared SHLP2 peptide. The rabbits were then boosted twice by the same SHLP2 peptide on day 14, 28 and were sacrificed on day 35 for all anti-serum collection. To sacrifice the mice, general anesthesia was induced by intraperitoneal injection of Zoletil (0.5 mg/10 g), followed by heart puncture for exsanguination for blood collection.

Human subject

Ethical approval was obtained from the Committee of the Yonsei University College of Medicine (4-2017-1168)⁴³ for the collection of human peripheral blood samples and performed in accordance with the Helsinki declaration. All participants provided written informed consent. The information of human subject used in study were listed in Supplementary Table 1.

Animals

All animal experiments and surgical procedure were approved by the Institutional Animal Care and Use Committee (IACUC) of the Avison Biomedical Research Center, Yonsei University. Male mice of 8–12 weeks of age were used in all experiments and housed in individual cages with a 12:12 h light–dark cycle (light automatically on/off at 08:00–20:00) at 22 \pm 1 $^{\circ}\text{C}$ and 55% humidity. Mice were fed with either regular chow diet (Lab Diet, 5053) or high fat diet (Research Diets, D12492) and provided with water *ad libitum*. For the experiments, C57BL/6j (JAX No. 000664)⁴⁴, C57BL/6j-*ob/ob* (SLC, Inc. Tokyo, Japan), C57BLKS/J-*db/db* (JAX No. 000662)⁴⁵, POMC-Cre (JAX No. 005965)²¹, AgRP-Ires-Cre (JAX No. 012899)²⁰, R26-tdTomato (JAX No. 007914)²², R26-hM4Di/mCitrine (JAX No. 026219)²⁴ mice were used. POMC-Cre mice were crossed with R26-tdTomato or R26-hM4Di/mCitrine mice to generate POMC-Cre/ R26-tdTomato (tdTomato^{POMC-Cre}) or POMC-Cre/ R26-hM4Di/mCitrine (hM4Di^{POMC-Cre}) mice. AgRP-Ires-Cre mice were crossed with R26-tdTomato mice to generate AgRP-Ires-Cre/ R26-tdTomato (tdTomato^{AgRP-Cre}).

Surgery

For intracerebroventricular (ICV) cannulation, mice were anesthetized by intraperitoneal injection (IP) of Zoletil (titelamine/zolazepam

30 mg/kg) and Rompun (xylazine 10 mg/kg), then placed onto a stereotaxic apparatus. After setting the ventricular coordinates, a permanent 26-gauge stainless steel cannula (Plastic one, Inc.) was implanted in the third ventricle (1.8 mm caudal to bregma, and 5.0 mm ventral to the sagittal sinus according to the Paxinos and Franklin's atlas) and secured to the skull surface using a dental acrylic (Vertex). Mice were individually housed and allowed to recover for at least 1 week. The angiotensin II-induced water consumption test was performed to confirm the position of the ICV cannulation. An immediate dipsogenic reaction within the first 10 min was observed in the animals with the correct cannula placement. Mice with no angiotensin II-induced thirst behavior were excluded from the experiments.

For pharmacogenetic studies to target the POMC neurons, pAAV-hSyn-DIO-hM4D(Gi)-mCherry (Addgene, 44362) or pAAV-hSyn-DIO-mCherry (AAV2) control (Addgene, 50459) were bilaterally injected into the hypothalamic ARC of 10-week-old POMC-cre mice. Mice were anesthetized using Zoletil/Rumpun and were placed into a stereotaxic apparatus (David Kopf Instruments, Kopf1900). The skull was exposed via a small incision, and a small burr hole was drilled. A Nanofil 10 μ L syringe with a 35 G blunt-end needle was inserted into the brain for virus delivery. Adenovirus injected via a syringe pump (KD Scientific) at a rate of 50 nL/min for 5 min. 0.25 μ L per injection site of ARC using appropriate coordinates: anteroposterior (AP), -1.8 mm; medio-lateral (ML), \pm 0.25 mm; dorso-ventral (DV), -5.7 mm. Two weeks following the virus injection, a cannula was implanted into the third ventricle and the angiotensin II-induced water consumption test was performed to confirm the correct cannula placement. Mice with incorrect stereotaxic injection outside the ARC were excluded from analysis after confirmation of mCherry expression.

SHLP2 injection

For IP injections, SHLP2 and control saline were administered daily at 2 mg/kg. After 3 weeks of injections, the body compositions were analyzed using Dual-energy X-ray absorptiometry (DEXA) system (InAnalyzer™, MEDIKORS) and metabolic assessments were performed.

For ICV injection, mice were handled daily for 3 days to minimize stress responses and administered with 3 μ g of SHLP2 or control saline followed with overnight fasting (18 h) and metabolic assessments were evaluated after 24 h of injection.

For chemogenetic inactivation of POMC neurons, mice were ICV administration of 1 μ g of CNO (Tocris, 4936). The metabolic study with SHLP2 or saline was performed 1 h after the CNO injection. Acute food intake was measured after ICV injection of Saline of SHLP2 followed with overnight fasting.

Metabolic phenotyping

Metabolic cage study was performed using the 12-channel PhenoMaster Home Cage System (TSE Systems) equipped with triple beam IR technology to assess indirect calorimetry, food and water consumption, oxygen consumption (VO_2), carbon dioxide production (VCO_2), and local motor activity^{46,47}. After acclimation for 48 h, physiological parameters were monitored for a 96-h recording period. Average metabolic parameters from three 24-h acquisition cycles were calculated and statistically analyzed. The relationship between energy expenditure and total body mass was normalized to either lean body mass or body weight^{0.75}. We used the latter because lean mass could not be measured due to the ICV cannula. Body fat and lean masses of mice were analyzed by a DEXA system (InAnalyzer™, MEDIKORS)⁴⁶. The DEXA system was calibrated in accordance with the operator's instructions before measurement and was set as the lower limit detection of 0.001 g/cm².

Rectal and skin temperature

Body temperatures were monitored after SHLP2 or saline ICV injections with 1-h pre-treatment of CNO at room temperature (RT). Rectal

and skin temperatures of mice were measured using a Thermalert TH-5 thermometer (Physitemp Instruments) with a small-diameter temperature probe or an FLIR-E5XT handheld infrared camera (FLIR Systems). Several infrared pictures were taken of the mice during the light phase while it was allowed to move freely in the house cage. Skin temperature was recorded by storing the temperature of the warmest pixel in thermal images.

Glucose and insulin tolerance tests

Glucose tolerance (GTT) and insulin tolerance (ITT) tests were performed in mice after 3 weeks of IP injection or 4 h of ICV injection of SHLP2. For GTT, mice were fasted overnight with water *ad libitum*. The ITT were performed under fed condition. The D-glucose (1 g/kg of body weight, Sigma-Aldrich, G8270) or insulin (1.2 U/kg of body weight, Humulin R, Eli Lilly) were administered by IP injection. Blood glucose levels were measured from a tail-nick venous blood using a handheld glucose monitor (Contour TS, Ascensia Diabetes Care). Blood glucose levels were measured before ($t = 0$) and after glucose or insulin injections at indicated time points.

Acute brain slice preparation

The 6- to 12-week-old tdTomato^{POMC-Cre} or tdTomato^{AgRP-Cre} or hM4Di^{POMC-Cre} mice were anesthetized with IP injections of Zoletil/Rumpun. Mice were rapidly perfused with ice-cold cutting artificial cerebrospinal fluid (aCSF) comprising of (in mM) 93.0 *N*-methyl-D-glucamine, 2.5 KCl, 1.2 NaH₂PO₄, 24.0 NaHCO₃, 20.0 HEPES, 7.5 Glucose, 5.0 Na-ascorbate, 3.0 Na-pyruvate, 10 MgSO₄ and 0.5 CaCl₂, with pH of 7.3-7.4 and an osmolality of 300-330 mOsm/kg. The brain was dissected and a block containing the hypothalamus was made. Two to three 250-300 μ m thick coronal slices containing the ARC of the hypothalamus were cut on 7000smz-2 Vibratome (Campden Instrument) in cold cutting aCSF. Slices were moved to carbogenated recording aCSF containing (in mM) 124.0 NaCl, 2.5 KCl, 1.2 NaH₂PO₄, 24.0 NaHCO₃, 5.0 HEPES, 5.0 Glucose, 2.0 MgSO₄ and 2.0 CaCl₂, pH 7.3-7.4, and osmolality 300-310 mOsm/kg. Slices were left to recover for 45 min at 35 °C, then at least 1 h at RT before any further experiments.

Slices were moved to a submerged-type recording chamber with continuous perfusion of carbogenated recording aCSF heated to 31 °C at a flow rate of approximately 2 mL/min. Tested compounds were added through bath perfusion. To block synaptic inputs, the aCSF contained 100 nM tetrodotoxin (TTX citrate; Tocris, 1069), 100 μ M picrotoxin (Sigma-Aldrich, P8390), 100 μ M D(-)-2-Amino-5-phosphopentanoic acid (D-AP-5; Tocris, 0106) and 20 μ M CNQX (CNQX-disodium; Tocris, 1045). To block ERK1/2 activation or PI3K signaling pathway, 10 μ M of PD98059 (Tocris, 1213) or 1 μ M of wortmannin (Tocris, 1232) was added to the bath solution for at least 30 min before any measurement. To test the effect of CNO on POMC neurons expressing the DREDD hM4Di receptor, 5 μ M of CNO were applied for 1 to 2 min.

Whole-cell patch-clamp recording

POMC or AgRP-expressing neurons in the ARC were identified with a brief exposure to epifluorescence on an upright microscope (Nikon FN1) using a 40X water-immersion objective and differential interference contrast optics. The pipette solution contains (in mM) 127 K-Methanesulfonate, 5 KCl, 10 HEPES, 0.3 EGTA, 4 Mg-ATP, 0.3 Na-GTP, and is of a pH adjusted to 7.3 with KOH and a 288 mOsm/kg osmolality. The patch pipettes have a resistance of 4-6 M Ω when filled with the pipette solution. Whole-cell configuration was achieved with brief negative pressure at a holding voltage of -50 mV. The basal resting membrane potential and firing rate were recorded for around 3 min after breaking in, and bath perfusion of SHLP2 was applied for 3 to 5 min. Neurons were classified as responsive if there was a change in resting membrane potential of at least 2 mV during the period of drug

application⁴⁸. The access resistance (R_a) was monitored throughout the experiment, and cells with a R_a of more than 35 M Ω were excluded from the analysis. Data were acquired at 10 kHz, filtered with a lowpass filter at 5 kHz and analyzed offline with Clampfit 10 (Molecular Devices). The calculated liquid junction potential was +9.55 mV and used to correct all data.

Hormone measurements

Serum insulin and leptin levels were measured by ELISA kits (Moringa Institute of Biological Science, M1104 and M1305, respectively) in accordance with the manufacturer's instructions.

For serum norepinephrine (NE), commercial ELISA kits (Labor Diagnostika Nord GmbH & Co., BA-E-5200) were used following the manufacturer's manual. Serum was extracted by using a cis-diol-specific affinity gel and acylated, then converted enzymatically before being quantitatively determined by a competitive enzyme immunoassay method.

Immunohistochemistry (IHC)

Whole brains were dissected out and post-fixed with 10% neutral buffered formalin overnight and dehydrated in 20% sucrose solution until the tissue sank to the bottom of the container. The brains were frozen-sectioned into 25 μ m slices in LEICA section system (Leica Biosystems, SM2010R) and stored in anti-freeze solution before used. Brain sections were washed and then incubated 30 min in 1X PBS containing 0.25% (v/v) Triton X-100 (PBT). Brain sections were blocked in 3% goat serum prepared in 0.1% PBT for 1 h at room temperature (RT) and then incubated overnight with c-Fos antibody (Cell Signaling, 2250, 1:1000) or DsRed antibody (TaKaRa, 632496, 1:200) or CXCR7 antibody (Proteintech, 20423-1-AP, 1:500) at 4 °C. Washed brain sections were incubated in the goat anti-rabbit secondary antibody with Alexa Fluor 488 (Invitrogen, A21206, 1:1000) or Alexa Fluor 594 (Invitrogen, A11012, 1:1000) prepared in PBT containing 3% goat serum. Sections were washed and mounted on glass slides. Brain slides were visualized using a LEICA fluorescence microscope (LEICA Corporation) or a confocal laser microscope (LSM700) with Cal Zeiss Zen 2.6 imaging software. c-Fos were counted using Fiji (image J2) 2.3.0 and Adobe Photochop CS6 software.

For UCPI staining, paraffin-embedded sections of formalin-fixed iBAT samples were mounted on a glass slide and incubated with UCPI primary antibody (Abcam, ab10983, 1:1000) overnight at 4 °C in a humidified chamber. The slides were washed 5 times with 1X PBS and then incubated with biotinylated donkey anti-rabbit IgG (Jackson ImmunoResearch, 711-065-152, 1:1000) for 2 h at RT, followed by an hour incubation in a solution of avidin-biotin complex (Vector, PK-6200). After 2 washes, the slides were stained with 3,3'-diaminobenzidine (DAB)-peroxidase substrate solution (0.04% DAB and 0.01% H₂O₂) in PBS for less than 2 min and were visualized by a Nikon Digital Camera DXM1200 microscope system (Nikon Corporation).

Cell culture

HEK293T cells (ATCC) were cultured in Dulbecco's modified Eagle medium (DMEM; Capricorn scientific) supplemented with 10% fetal bovine serum (FBS; Corning), 100 U/mL penicillin, and 100 μ g/mL streptomycin (Gibco). Cells were maintained at 37 °C and in a humidified, 5% CO₂ atmosphere.

Immuno-dot blot assay

The immuno-dot blot assay was performed by using the human and mice serum or mouse CSF. 0.2 μ m nitrocellulose membranes were activated with ultrapure water (Invitrogen, 10977015), and 2 μ L of samples were spotted on a membrane and dried for 30 mins at RT. The membrane was blocked in 5% BSA prepared in 1X Tris Buffered Saline-0.1% Tween 20 (TBST) for 1 h before being overnight incubated with anti-SHLP2 at 4 °C. Membranes were washed 3 times with 1X TBST,

then incubated with anti-rabbit IgG (Invitrogen, 31460, 1:3000). The membranes were washed and visualized using the ImageQuant™ LAS 4000 (GE Healthcare Life Science). Blot densitometry was measured using ImageJ software (NIH Image). To quantitate the immuno-dot blot assay results, we prepared controls (total protein level stained by amido black), and subsequently established a calibration figure for each run of the assay.

Pull-down assay

Ten μ g of the plasmid DNA pEGFP-N1 (Clontech) or pcDNA3.1-Zeo-hCXCR7-sGFP (a gift of Prof. Jong-Ilk Hwang, Korea University)⁴⁹ were transfected to HEK293T cells using Lipofectamine 2000 (Invitrogen, 11668019) according to the manufacturer's instruction. After the transfections for 24 h, cells were trypsinized and collected in ice-cold 1X PBS. The cell suspension was incubated with either 10 μ M Biotinylated SHLP2 or Biotin (Sigma-Aldrich, B4501) for 30 min at 4 °C, then cross-linked by 1 mM of disuccinimidyl suberate (DSS; Thermo Scientific) for 30 min. Cells were washed with Tris-buffered saline (pH 7.5) to quench and remove excess cross-linkers and lysed in RIPA buffer. To capture the biotinylated peptide-receptor complex, streptavidin agarose beads (Sigma-Aldrich, 21655) were added and incubated at 4 °C for 4 h. Beads were collected by centrifugation and washed with RIPA buffer. Elution was performed with 1% SDS and 100 mM Dithiothreitol (DTT) for 1 h at RT. Fractions were subjected to routine polyacrylamide gel electrophoresis and immunoblotting.

Western blot

Tissue or cell lysates were prepared in RIPA buffer as previously describe⁴⁶. Equal protein amounts were to SDS-PAGE electrophoresis. Separated proteins on gels were then transferred onto PVDF membranes, blocked in 5% skim milk for 1 h before being incubated overnight at 4 °C. In the following primary antibodies: UCPI (Abcam, ab10983, 1:10,000), p-p38 MAPK (Cell Signaling, 4511, 1:1000), p-ERK (Cell Signaling, 9101, 1:1000), ERK (Cell Signaling, 9102, 1:1000), p-CREB (Cell Signaling, 9196, 1:1000), GFP (Sigma-Aldrich, G1544, 1:3000) and α -tubulin (Developmental Studies Hybridoma Bank, 12G10, 1:5000). Membranes were washed with 1X TBST and then were incubated with anti-rabbit IgG (Invitrogen, 31460, 1:3000) or anti-mouse IgG (Invitrogen, 62-6520, 1:2000). Blots were visualized by ImageQuant™ LAS 4000 or X-ray film. Blots densitometry were measured using ImageJ software.

Quantitative PCR (q-PCR)

Total RNA was extracted from homogenized tissues using the TRizol reagent (Thermo Scientific) and equal amounts of total RNA were reversely transcribed into cDNA using ReverTra Ace qPCR RT Master Mix with gDNA Remover (Toyobo, FSQ-301). The cDNA templates were then amplified and quantified by the BioRad CFX Real-Time PCR system (BioRad) using iQ™ SYBR® Green Supermix (BioRad, 1708880).

To measure mitochondrial DNA content, total DNA from iBAT samples was extracted using AccuPrep® Genomic DNA Extraction Kit (Bioneer, K-3032) according to the manufacturer's instructions. Total DNA from each sample was amplified using primers specific for the mitochondrial cytochrome C oxidase subunit 2 (*Cox2*) gene and the ribosomal protein s18 (*Rps18*) nuclear gene. The primer sequences used in qPCR were listed in the Supplementary Table 2.

Internalization assay

HEK293T cells were seeded onto the glass coverslips coated with Poly-L-Lysine and transfected with 1 μ g of pcDNA3.1-Zeo-CXCR7-SGFP or pcDNA31-Zeo-CXCR4-SGFP. After 24 h, cells are treated with 10 μ M SHLP2 or DMSO at indicated time points. Cells were fixed with cold methanol and incubated with anti-GFP antibody overnight at 4 °C. The GFP were visualized with anti-rabbit-AlexaFluor-488 secondary antibody, and the nuclei were stained with DAPI. Cells were examined

using laser-scanning microscope LSM700. At least 100 cells were counted from each replication.

GPCR screening

The GPCR profiling was performed using PathHunter GPCRmax Arrestin recruitment assay with 168 known GPCRs provided by DiscoverX (Eurofins). This assay utilized Chinese Hamster Ovary CHO-K1 cells expressing GPCR tagged with ProLink (PK) and β -Arrestin2 tagged with a deletion mutant of β -galactosidase as an enzyme acceptor. Upon the binding of the ligand to the GPCR, the recruitment of tagged β -Arrestin2 to the GPCR causes the complementation of a functional β -galactosidase, hydrolyzing a chemiluminescence substrate. The assay was performed with known ligands in agonist and antagonist modes, with data presented as:

$$\% \text{Activity (agonist)} = 100\% \times \frac{\text{Mean RLU (SHLP2)} - \text{Mean RLU (vehicle control)}}{\text{Mean MAX RLU (control ligand)} - \text{Mean RLU (vehicle control)}}$$

and

$$\% \text{Activity (antagonist)} = 100\% \times \left(1 - \frac{\text{Mean RLU (SHLP2)} - \text{Mean RLU (vehicle control)}}{\text{Mean MAX RLU (control ligand)} - \text{Mean RLU (vehicle control)}} \right)$$

The dose response (EC_{50}) was built using a 10-point curve and fit to a Hill Equation.

Nanoluc-complementation based β -Arrestin2 recruitment assay

The recruitment assay was performed based on Nano-luciferase⁴⁹. The vectors (50 ng; gift of Prof. Jong-Ik Hwang, Korea University) encoding human CXCR7, CXCR4, and β -Arrestin2 tagged with SmbiIT and LgBiIT under Ubiquitin C promoter⁴⁹ were transfected into HEK293T cells in a 96-well clear bottom culture plate using Lipofectamine 2000 according to the manufacturer's protocol. Cells were washed three times with an assay buffer containing (in mM) 140 NaCl, 2.5 KCl, 10 Glucose, 5 HEPES, 2 CaCl₂, and 2 MgSO₄, pH 7.4 after 24 h. Cells were then incubated with 5 μ M Coelenterazine-h (Promega, S201) in the assay buffer for 30 min in the dark, and luminescence was measured at 35 °C in the Victor Nivo Multimode Plate reader (PerkinElmer). The background luminescence was measured for at least 10 min before the addition of ligands, and signals were monitored for at least 60 min after the application of SHLP2 or recombinant mouse CXCL12 (R&D systems, 460-SD-010/CF). The specificity of SHLP2 β -Arrestin2 recruitment through CXCR7 was also confirmed through the assay with CXCR4. Luminescent signals were collected through a 700 nm-IR filter and data were shown as light counts per each cycle of measurement.

Statistics

Prism 8.0 (GraphPad Software) was used for all the statistical analyses and making graphs. Data are represented as mean \pm SEM and a p -value less than 0.05 was defined as a statistically significant difference. Unpaired 2-tailed Student's t tests or one-way analysis of variance (ANOVA) with Tukey's post-tests were used to determine the statistical significance between two or multiple groups, respectively. Two-way ANOVA with the Bonferroni post-tests was used to determine the statistical significance between multiple groups with two independent variables. Detailed statistical test(s) used and corresponding p -value are described in figure legends. Differences were considered statistically significant at * $P < 0.05$, ** $P < 0.01$; *** $P < 0.001$.

Reporting summary

Further information on research design is available in the Nature Portfolio Reporting Summary linked to this article.

Data availability

The datasets generated in this study are available in the Supplementary Information/Source Data file. Supplementary Information/Source data is included with this paper.

References

1. Taanman, J. W. The mitochondrial genome: structure, transcription, translation and replication. *Biochim. Biophys. Acta* **1410**, 103–123 (1999).
2. Mercer, T. R. et al. The human mitochondrial transcriptome. *Cell* **146**, 645–658 (2011).
3. Merry, T. L. et al. Mitochondrial-derived peptides in energy metabolism. *Am. J. Physiol. Endocrinol. Metab.* **319**, E659–E666 (2020).
4. Cobb, L. J. et al. Naturally occurring mitochondrial-derived peptides are age-dependent regulators of apoptosis, insulin sensitivity, and inflammatory markers. *Aging (Albany NY)* **8**, 796–809 (2016).
5. Lee, C., Yen, K. & Cohen, P. Humanin: a harbinger of mitochondrial-derived peptides. *Trends Endocrinol. Metab.* **24**, 222–228 (2013).
6. Hashimoto, Y. et al. Detailed characterization of neuroprotection by a rescue factor humanin against various Alzheimer's disease-relevant insults. *J. Neurosci.* **21**, 9235–9245 (2001).
7. Hashimoto, Y. et al. A rescue factor abolishing neuronal cell death by a wide spectrum of familial Alzheimer's disease genes and Abeta. *Proc. Natl. Acad. Sci. USA.* **98**, 6336–6341 (2001).
8. Yen, K. et al. The mitochondrial derived peptide humanin is a regulator of lifespan and healthspan. *Aging (Albany N. Y.)* **12**, 11185–11199 (2020).
9. Lee, C. et al. The mitochondrial-derived peptide MOTS-c promotes metabolic homeostasis and reduces obesity and insulin resistance. *Cell Metab.* **21**, 443–454 (2015).
10. Kim, K. H., Son, J. M., Benayoun, B. A. & Lee, C. The mitochondrial-encoded peptide MOTS-c translocates to the nucleus to regulate nuclear gene expression in response to metabolic stress. *Cell Metab.* **28**, 516–524.e517 (2018).
11. Reynolds, J. C. et al. MOTS-c is an exercise-induced mitochondrial-encoded regulator of age-dependent physical decline and muscle homeostasis. *Nat. Commun.* **12**, 470 (2021).
12. Nashine, S., Cohen, P., Nesburn, A. B., Kuppermann, B. D. & Kenney, M. C. Characterizing the protective effects of SHLP2, a mitochondrial-derived peptide, in macular degeneration. *Sci. Rep.* **8**, 15175 (2018).
13. Mehta, H. H. et al. Metabolomic profile of diet-induced obesity mice in response to humanin and small humanin-like peptide 2 treatment. *Metabolomics* **15**, 88 (2019).
14. Betz, M. J. & Enerback, S. Targeting thermogenesis in brown fat and muscle to treat obesity and metabolic disease. *Nat. Rev. Endocrinol.* **14**, 77–87 (2018).
15. Harms, M. & Seale, P. Brown and beige fat: development, function and therapeutic potential. *Nat. Med.* **19**, 1252–1263 (2013).
16. Tran, L. T. et al. Hypothalamic control of energy expenditure and thermogenesis. *Exp. Mol. Med.* **54**, 358–369 (2022).
17. Yang, D. J., Hong, J. & Kim, K. W. Hypothalamic primary cilium: a hub for metabolic homeostasis. *Exp. Mol. Med.* **53**, 1109–1115 (2021).
18. Ellacott, K. L. & Cone, R. D. The central melanocortin system and the integration of short- and long-term regulators of energy homeostasis. *Recent Prog. Horm. Res.* **59**, 395–408 (2004).
19. Yeo, G. S. H. et al. The melanocortin pathway and energy homeostasis: from discovery to obesity therapy. *Mol. Metab.* **48**, 101206 (2021).
20. Tong, Q., Ye, C. P., Jones, J. E., Elmquist, J. K. & Lowell, B. B. Synaptic release of GABA by AgRP neurons is required for normal regulation of energy balance. *Nat. Neurosci.* **11**, 998–1000 (2008).

21. Balthasar, N. et al. Leptin receptor signaling in POMC neurons is required for normal body weight homeostasis. *Neuron* **42**, 983–991 (2004).
22. Madisen, L. et al. A robust and high-throughput Cre reporting and characterization system for the whole mouse brain. *Nat. Neurosci.* **13**, 133–140 (2010).
23. van den Pol, A. N. et al. Neuromedin B and gastrin-releasing peptide excite arcuate nucleus neuropeptide Y neurons in a novel transgenic mouse expressing strong Renilla green fluorescent protein in NPY neurons. *J. Neurosci.* **29**, 4622–4639 (2009).
24. Zhu, H. et al. Cre-dependent DREADD (Designer Receptors Exclusively Activated by Designer Drugs) mice. *Genesis* **54**, 439–446 (2016).
25. Mullican, S. E. et al. GFRAL is the receptor for GDF15 and the ligand promotes weight loss in mice and nonhuman primates. *Nat. Med.* **23**, 1150–1157 (2017).
26. Dixon, A. S. et al. NanoLuc complementation reporter optimized for accurate measurement of protein interactions in cells. *ACS Chem. Biol.* **11**, 400–408 (2016).
27. Tripathi, V., Kumar, R., Dinda, A. K., Kaur, J. & Luthra, K. CXCL12-CXCR7 signaling activates ERK and Akt pathways in human choriocarcinoma cells. *Cell Commun. Adhes.* **21**, 221–228 (2014).
28. Decaillot, F. M. et al. CXCR7/CXCR4 heterodimer constitutively recruits beta-arrestin to enhance cell migration. *J. Biol. Chem.* **286**, 32188–32197 (2011).
29. Burns, J. M. et al. A novel chemokine receptor for SDF-1 and I-TAC involved in cell survival, cell adhesion, and tumor development. *J. Exp. Med.* **203**, 2201–2213 (2006).
30. Zhang, J. et al. ERK1/2 mediates glucose-regulated POMC gene expression in hypothalamic neurons. *J. Mol. Endocrinol.* **54**, 125–135 (2015).
31. Cui, H., Cai, F. & Belsham, D. D. Leptin signaling in neurotensin neurons involves STAT, MAP kinases ERK1/2, and p38 through c-Fos and ATF1. *FASEB J.* **20**, 2654–2656 (2006).
32. Plum, L. et al. Enhanced PIP3 signaling in POMC neurons causes KATP channel activation and leads to diet-sensitive obesity. *J. Clin. Invest.* **116**, 1886–1901 (2006).
33. Jang, J. Y., Blum, A., Liu, J. & Finkel, T. The role of mitochondria in aging. *J. Clin. Invest.* **128**, 3662–3670 (2018).
34. Jelenik, T. & Roden, M. Mitochondrial plasticity in obesity and diabetes mellitus. *Antioxid Redox Signal* **19**, 258–268 (2013).
35. Prasun, P. Mitochondrial dysfunction in metabolic syndrome. *Biochim. Biophys. Acta Mol. Basis Dis.* **1866**, 165838 (2020).
36. Yin, Y. et al. The mitochondrial-derived peptide MOTS-c relieves hyperglycemia and insulin resistance in gestational diabetes mellitus. *Pharmacol. Res.* **175**, 105987 (2022).
37. Lam, B. Y. H. et al. Heterogeneity of hypothalamic pro-opiomelanocortin-expressing neurons revealed by single-cell RNA sequencing. *Mol. Metab.* **6**, 383–392 (2017).
38. Biglari, N. et al. Functionally distinct POMC-expressing neuron subpopulations in hypothalamus revealed by intersectional targeting. *Nat. Neurosci.* **24**, 913–929 (2021).
39. Williams, K. W. et al. Segregation of acute leptin and insulin effects in distinct populations of arcuate pro-opiomelanocortin neurons. *J. Neurosci.* **30**, 2472–2479 (2010).
40. Lu, S. C. & Akanji, A. O. Leptin, obesity, and hypertension: a review of pathogenetic mechanisms. *Metab. Syndr. Relat. Disord.* **18**, 399–405 (2020).
41. Eshingdrelo, H. et al. ERK and beta-arrestin interaction: a converging point of signaling pathways for multiple types of cell surface receptors. *J. Biomol. Screen.* **20**, 341–349 (2015).
42. Zhao, Y. G. et al. A novel mechanism by which SDF-1 beta protects cardiac cells from palmitate-induced endoplasmic reticulum stress and apoptosis via CXCR7 and AMPK/p38 MAPK-mediated interleukin-6 generation. *Diabetes* **62**, 2545–2558 (2013).
43. Cho, Y. et al. Ezetimibe combination therapy with statin for non-alcoholic fatty liver disease: an open-label randomized controlled trial (ESSENTIAL study). *BMC Med.* **20**, 93 (2022).
44. Paigen, B., Morrow, A., Brandon, C., Mitchell, D. & Holmes, P. Variation in susceptibility to atherosclerosis among inbred strains of mice. *Atherosclerosis* **57**, 65–73 (1985).
45. Mao, H. Z., Roussos, E. T. & Péterfy, M. Genetic analysis of the diabetes-prone C57BLKS/J mouse strain reveals genetic contribution from multiple strains. *Biochim. Biophys. Acta* **1762**, 440–446 (2006).
46. Sun, J. S. et al. Ventromedial hypothalamic primary cilia control energy and skeletal homeostasis. *J. Clin. Invest.* **131**, e138107 (2021).
47. Kim, K. W. et al. FOXO1 in the ventromedial hypothalamus regulates energy balance. *J. Clin. Invest.* **122**, 2578–2589 (2012).
48. He, Z. et al. Direct and indirect effects of liraglutide on hypothalamic POMC and NPY/AgRP neurons - Implications for energy balance and glucose control. *Mol. Metab.* **28**, 120–134 (2019).
49. Nguyen, H. T. et al. CXCR7: a beta-arrestin-biased receptor that potentiates cell migration and recruits beta-arrestin2 exclusively through Gbetagamma subunits and GRK2. *Cell Biosci.* **10**, 134 (2020).

Acknowledgements

This research was supported by the Korea Drug Development Fund, funded by the Ministry of Science and ICT, the Ministry of Trade, Industry, and Energy, and the Ministry of Health and Welfare (HN22C0645, Republic of Korea). The research was also supported by the National Research Foundation of Korea (2021R1A2C4002011 and RS-2023-00217709 for K.W.K.; 2021R1I1A1A01049540 for Y.-H.C.) and the Korea Health Industry Development Institute (Korea Health Technology R&D Project: HR22C141102 for K.W.K.). This work was also partly supported by the KBRI basic research program (23-BR-01-02 for H.-H.L.).

Author contributions

K.S.K. performed experiments, analyzed data, wrote, and finalized the manuscript. T.L.T. performed whole-cell patch-clamp recording and edited the manuscript. C.N.K., H.J.C., M.H.C., C.H.C., J.M.H., and H.H.L. assisted with experimental design and analysis. H.J.J. and Y.H.L. provide human samples. Y.H.C. and D.M.S. reviewed and edited the manuscript. K.W.K. conceptualized the research, edited, and finalized the manuscript.

Competing interests

The authors declare no competing interests.

Additional information

Supplementary information The online version contains supplementary material available at <https://doi.org/10.1038/s41467-023-40082-7>.

Correspondence and requests for materials should be addressed to Ki Woo Kim.

Peer review information *Nature Communications* thanks Jose Donato Jr, Ichiro Sakata, Young-Bum Kim and the other, anonymous, reviewers for their contribution to the peer review of this work. A peer review file is available.

Reprints and permissions information is available at <http://www.nature.com/reprints>

Publisher's note Springer Nature remains neutral with regard to jurisdictional claims in published maps and institutional affiliations.

Open Access This article is licensed under a Creative Commons Attribution 4.0 International License, which permits use, sharing, adaptation, distribution and reproduction in any medium or format, as long as you give appropriate credit to the original author(s) and the source, provide a link to the Creative Commons licence, and indicate if changes were made. The images or other third party material in this article are included in the article's Creative Commons licence, unless indicated otherwise in a credit line to the material. If material is not included in the article's Creative Commons licence and your intended use is not permitted by statutory regulation or exceeds the permitted use, you will need to obtain permission directly from the copyright holder. To view a copy of this licence, visit <http://creativecommons.org/licenses/by/4.0/>.

© The Author(s) 2023, corrected publication 2023